UCLA
UCLA Previously Published Works

Title
Performing radiosynthesis in microvolumes to maximize molar activity of tracers for positron emission tomography

Permalink
https://escholarship.org/uc/item/4z99v1zb

Journal
Communications Chemistry, 1(1)

ISSN
2399-3669

Authors
Sergeev, Maxim
Lazari, Mark
Morgia, Federica
et al.

Publication Date
2018

DOI
10.1038/s42004-018-0009-z

Peer reviewed

eScholarship.org Powered by the California Digital Library
University of California

Author Manuscript
Author Manuscript
Author Manuscript
Author Manuscript

HHS Public Access
Author manuscript
Commun Chem. Author manuscript; available in PMC 2021 July 20.

Published in final edited form as:
Commun Chem. 2018 ; 1(1): . doi:10.1038/s42004-018-0009-z.

Performing radiosynthesis in microvolumes to maximize molar activity of tracers for positron emission tomography

Maxim E. Sergeev[1,2,§], **Mark Lazari**[1,2,3], **Federica Morgia**[1,2], **Jeffrey Collins**[1,2], **Muhammad Rashed Javed**[1,2], **Olga Sergeeva**[1,2], **Jason Jones**[4], **Michael E. Phelps**[1,2,5], **Jason T. Lee**[1,2,5], **Pei Yuin Keng**[1,2,5,*], **R. Michael van Dam**[1,2,3,4,5,*]

[1]Crump Institute for Molecular Imaging, University of California, Los Angeles (UCLA), 570 Westwood Plaza, Los Angeles, CA, USA, 90095

[2]Department of Molecular & Medical Pharmacology, David Geffen School of Medicine, University of California, Los Angeles (UCLA), 650 Charles E. Young Dr. S., Los Angeles, CA, USA, 90095

[3]Department of Bioengineering, Henry Samueli School of Engineering and Applied Science, UCLA, Los Angeles, CA, USA

[4]Physics and Biology in Medicine Interdepartmental Graduate Program, David Geffen School of Medicine, UCLA, Los Angeles, CA, USA

[5]Jonsson Comprehensive Cancer Center, 8-684 Factor Building, UCLA, Los Angeles, CA, USA, 90095

Abstract

Positron emission tomography (PET) is a molecular diagnostic imaging technology to quantitatively visualize biological processes *in vivo*. For many applications, including imaging of low tissue density targets (e.g. neuroreceptors), imaging in small animals, and evaluation of novel tracers, the injected PET tracer must be produced with high molar activity to ensure low occupancy of biological targets and avoid pharmacologic effects. Additionally, high molar activity is essential for tracers with lengthy syntheses or tracers transported to distant imaging sites. We show that radiosynthesis of PET tracers in microliter volumes instead of conventional milliliter volumes results in substantially increased molar activity, and we identify the most relevant variables affecting this parameter. Furthermore, using the PET tracer [^{18}F]fallypride, we illustrate that molar activity can have a significant impact on biodistribution. With full automation,

*Corresponding authors: peiyuinkeng@gmail.com and mvandam@mednet.ucla.edu.
§Current address: Department of Radiology, University Hospitals Cleveland Medical Center, 11000 Euclid Ave., Cleveland, OH, USA, 44106

Author Contributions
MES, ML, JTL, PYK, and RMV conceived and designed the experiments; MES, ML, FM, JC, MRJ, OS, and JJ performed the experiments; MES, MS, FM, JTL, PYK and RMV analyzed data; MES, MEP, JTL, PYK, and RMV wrote the manuscript with input from all authors.

Competing Interests
Drs. van Dam and Phelps are founders of Sofie Biosciences, Inc., Dr. Phelps is a board member of Sofie Biosciences, and Drs. van Dam and Keng are consultants to Sofie Biosciences. The Regents of the University of California have licensed technology to Sofie Biosciences that was invented by Drs. van Dam, Keng, and Lazari, and have taken equity in Sofie Biosciences as part of the licensing transaction.

Data availability
All data generated or analyzed during this study are included in this published article (and its supplementary information files).

Author Manuscript Author Manuscript Author Manuscript Author Manuscript

microdroplet platforms could provide a means for radiochemists to routinely, conveniently, and safely produce PET tracers with high molar activity.

Positron emission tomography (PET) is an effective *in vivo* molecular imaging technology in clinical care, preclinical and clinical research, and drug discovery[1–5]. PET applications span a broad range of medical fields, including oncology, cardiology, immunology, and neurology. In the latter, for example, PET is used in the diagnosis and monitoring of neurodegenerative disorders[6], and is a vital tool in the discovery and development of novel therapeutics by enabling *in situ* measurements of drug target occupancy, binding kinetics, etc.[7]. Based on the principles of "tracer kinetics", PET enables measurements of biological processes such as receptor occupancy, cell proliferation, metabolism, apoptosis, and gene expression, quantification of their temporal changes, and identification of their roles in the mechanisms of disease without perturbing the underlying biology[8,9]. While PET tracers have been developed incorporating various radionuclides[10], those labeled with fluorine-18 are of particular interest due to the wide availability of this radionuclide and its favorable physical and chemical properties[11].

During synthesis of PET tracers, inevitable contamination by sources of non-radioactive [^{19}F]fluoride leads to a final product comprising a mixture of ^{18}F- and ^{19}F-labeled molecules, of which only the former are detectable by the PET scanner. Molar activity (A_m; commonly referred to as 'specific activity') describes the ratio of the radioactivity (i.e., quantity of ^{18}F-labeled molecules) to the total quantity of radioactive plus non-radioactive (i.e., ^{19}F-labeled) molecules[12–14]. High A_m of PET tracers is critical for many applications[15–17]: it minimizes occupancy when imaging low tissue density targets (e.g. neuroreceptors)[5,18–21], facilitates PET "microdosing" studies to evaluate the pharmacokinetics of novel drug compounds[22–25], extends the distance/time over which tracers can be transported to the imaging site[26], and is critical in preclinical research, where much higher concentrations of the tracer per mass of the animal must be injected (compared to humans) to achieve sufficient signal-to-noise ratio[19,20,27].

The theoretical maximum A_m of a radiofluorinated tracer is A_m^{max} = 1710 Ci/μmol [63.3 TBq/μmol] (i.e. all molecules are labeled with ^{18}F). However, reported A_m values are most typically in the 0.5–1.0 Ci/μmol [19–37 GBq/μmol] range (for nucleophilic radiofluorination)[26], though there is considerable variation[28] and a few reports of significantly higher A_m. Though there is not a consensus on what constitutes "high" A_m, we consider values >5 Ci/μmol [>185 GBq/μmol] to be "high". The discrepancy of three orders of magnitude between typical and maximum theoretical A_m can be attributed to [^{19}F]fluoride contamination in the radioisotope solution (i.e. from cyclotron production and delivery process) and/or from the radiosynthesis process itself (i.e. from reagents and/or synthesis apparatus). Since [^{18}F]fluoride and [^{19}F]fluoride have the same reactivity, both are incorporated into the precursor nearly in proportion to their abundance. Thus, the molar activity of a tracer can be expressed as:

$$A_m = A_m^{max}\left(\frac{{}^{18}F_c}{{}^{18}F_c + {}^{19}F_c + {}^{19}F_s}\right), \qquad \text{Equation 1}$$

Author Manuscript Author Manuscript Author Manuscript Author Manuscript

where $^{18}F_c$ is the number of [^{18}F]fluoride ions from the cyclotron, $^{19}F_c$ is the number of [^{19}F]fluoride ions from the cyclotron, and $^{19}F_s$ is the number of [^{19}F]fluoride ions from the synthesis process.

The typical strategy to increase A_m is to start with a higher amount of radioactivity (e.g. >1 Ci [>37 GBq]), thus increasing the numerator in Equation 1. In this approach, A_m > 20 Ci/µmol [>740 GBq/µmol] at end of synthesis (EOS) has been reported from 5 Ci [185 GBq][29,30], and unusually high A_m values of 130–160 Ci/µmol [4.7–5.9 TBq/µmol] at EOS were recently reported starting with ~6 Ci [220 GBq][31]. However, the use of such large amounts of radioactivity poses safety challenges in production and handling of the tracer, and can lead to significant radiolysis of the product[32]. Furthermore, the costs associated with using higher amounts of radioactivity may be difficult to justify if the goal is only to perform a small number of patient scans or to perform preclinical imaging. As an aside, another approach for increasing molar activity that isn't reflected in Equation 1 is the addition of multiple labeling sites per tracer molecule[16]. Using trifluoroborate derivatives, tripling of molar activity has been reported[33].

Reducing the amount of ^{19}F-contamination (i.e. $^{19}F_c$ and $^{19}F_s$ in Equation 1) is another strategy to improve A_m. Contamination present in the [^{18}F]fluoride solution after cyclotron bombardment can be characterized by:

$$A_m^{isotope} = A_m^{max}\left(\frac{^{18}F_c}{^{18}F_c + {}^{19}F_c}\right). \qquad \text{Equation 2}$$

Very high values of $A_m^{isotope}$ have been reported after optimization of cyclotron bombardment conditions (140 Ci/µmol [5 TBq/µmol] at EOB)[34] or processes related to loading and cleaning the [^{18}O]water target (1200 Ci/µmol [44 TBq/µmol] at EOB)[35]. However, it has been remarked that typical values are generally closer to the range of 10 Ci/µmol [370 GBq/µmol] at EOB[15] or 15–30 Ci/µmol [560–1100 GBq/µmol] at EOB[17,36]. Though $^{19}F_C$ can likely be reduced (and $A_m^{isotope}$ increased) for most cyclotrons, most radiochemists will not have control over this aspect of the tracer production. Contamination from the synthesis process ($^{19}F_s$) is generally even more significant and thus dominates the molar activity of the final tracer. In one study, radiolysis of Teflon was found to be a major source, with 90–95% reduction of contamination by avoiding Teflon (tubing, stir bars, etc.)[37]. Other sources of contamination include reagents (such as K_2CO_3, solvents, etc.)[38], and anion exchange cartridges (e.g. quaternary methylammonium, QMA) that are often used in the first step of ^{18}F-radiosyntheses[39].

We hypothesize that ^{19}F-contamination could be significantly decreased (and A_m increased) by replacing conventional radiochemistry approaches with microfluidic chips, due to orders of magnitude reduction in volumes and surface areas. Recently, droplet-based radiochemistry systems operating at the microliter scale have been developed[40,41]. Despite the small volumes, these chips can produce clinically-relevant amounts of PET tracers by pre-concentrating the radioisotope[42]. A few preliminary results have suggested that A_m of tracers produced with this platform may be significantly higher than macroscale

Author Manuscript Author Manuscript Author Manuscript Author Manuscript

methods[40,43–46]. Here, we report on a comprehensive study of these differences in A_m, comparing radiosyntheses of two model compounds performed at the micro- and macroscales. We observed interesting trends that shed light on the relative magnitude of the various contributions of ^{19}F-contamination. Microscale radiochemistry, it turns out, provides intrinsic advantages compared to conventional methods and could provide a means for consistently achieving high A_m without requiring the high starting activities that are necessary in macroscale processes.

Results

Factors affecting molar activity

Micro- and macroscale radiosynthesis were compared using two model precursors: 1,4-dinitrobenzene for aromatic fluorination leading to 1-[^{18}F]fluoro-4-nitrobenzene ([^{18}F]FNB), and tosyl-fallypride for aliphatic fluorination leading to [^{18}F]fallypride, a tracer for dopamine D2/D3 receptors (Figure 1). The microscale synthesis was performed on a microdroplet synthesis platform (Figure 2), and the macroscale synthesis, with a commercial synthesizer (ELIXYS, Sofie Biosciences, Inc.). The experimental design is illustrated in Figure 3. To facilitate comparisons among different experiments, molar activity values in the following sections have been corrected to end of bombardment (EOB).

Effect of reaction volume

Suspecting that increasing amount of reagents (i.e., precursor, base, phase transfer catalyst) would increase [^{19}F]fluoride contamination, we performed experiments in which the amount of [^{18}F]fluoride/[^{18}O]H_2O was held constant, but the amount of all reagents was varied (proportionally). The amount of base / phase transfer catalyst was varied by adding different volumes of the stock solutions during the [^{18}F]fluoride drying process, and the amount of precursor was varied in proportion by adding different volumes of the stock solution. Indeed, macroscale syntheses performed with increasing reaction volumes from 0.1 to 3.0 mL showed decreasing molar activity (Figure 4a). For example, for [^{18}F]FNB, A_m resulting from 0.1 mL reaction volume was nearly 10x higher than for the 3.0 mL reaction, i.e., 0.41 ± 0.04 Ci/μmol [15.2 ± 1.5 GBq/μmol] (n=3) *vs.* 0.04 ± 0.03 Ci/μmol [1.5 ± 1.1 GBq/μmol] (n=3), respectively. The same synthesis (starting with similar amount of radioactivity) in the microchip produced much higher A_m, 22.7 ± 0.6 Ci/μmol [840 ± 22 GBq/μmol] (n=12), and A_m was nearly constant despite fluorination volume variation from 2 to 8 μL (Figure 4b). For [^{18}F]fallypride, A_m was also found to be nearly constant (18.2 ± 0.4 Ci/μmol [673 ± 15 GBq/μmol], n=12) in microscale volumes from 2 to 8 μL (Figure 4b). Though variation in A_m of [^{18}F]fallypride at the macroscale was not systematically measured as a function of reaction volume, we noted that A_m for the synthesis at 0.5 mL scale was significantly lower (i.e., 0.9±0.05 Ci/μmol [33 ± 2 GBq/μmol]; n=3) than the chip results. These data demonstrate that reagents are the dominant source of ^{19}F-contamination at the macroscale, but are negligible relative to other sources at the microscale.

Though not related to molar activity, it is interesting to note that the decay-corrected radiochemical conversion of [^{18}F]fluoride into ^{18}F-labeled tracer in macro- and microscales (as measured by radio-TLC) were similar, and remained relatively constant across all

Author Manuscript Author Manuscript Author Manuscript Author Manuscript

volumes tested. Conversion was 67 ± 9% (n=11) at the macroscale and 54 ± 14% (n=12) at the microscale for [^{18}F]FNB, and 77 ± 1% (n=3) and 71 ± 2% (n=12), respectively, for [^{18}F]fallypride. Despite varying reaction volume at each synthesis scale, the conversion exhibited relatively little variation, perhaps due to the use of identical reagent concentrations.

Effect of starting radioactivity

Increasing the amount of the radioisotope is known to increase the molar activity at the macroscale, which is the rationale for using high starting radioactivities when producing a tracer with high A_m [29,30]. We compared the molar activity for both [^{18}F]FNB and [^{18}F]fallypride syntheses at the macroscale, starting from different radioactivities (8 to 360 mCi [0.3–13.3 GBq]) while maintaining a constant reaction volume (0.5 mL). A linear relationship between A_m and starting activity for both tracers was observed (Figure 4c). Comparative experiments were then conducted in microscale on-chip syntheses with fixed reaction volume (4 μL). Interestingly, A_m was relatively constant for both tracers (~20–25 Ci/μmol [740–930 GBq/μmol]), despite a wide range of starting radioactivities used (25 – 525 mCi [0.9 – 19.4 GBq]) (Figure 4c).

An interpretation for these results is depicted in Figure 5. Because the starting radioactivity was varied by adding different volumes of the [^{18}F]fluoride solution from the cyclotron, increasing the starting radioactivity therefore also increases the cyclotron source of ^{19}F-contamination. At the macroscale, we concluded above that reagents are the dominant source of ^{19}F-contamination; thus, even as starting activity is increased, we expect the associated increase in ^{19}F-contamination from the cyclotron to be negligible in comparison. Equation 1 then becomes $A_m \approx A_m^{max}\,[^{18}F_C / (^{18}F_C + {}^{19}F_S)] \approx A_m^{max}\,(^{18}F_C/^{19}F_S)$. (The second approximation is made since the number of fluorine-19 typical far outnumbers the number of fluorine-18 ions.) This equation describes a linear dependence of molar activity on the amount of [^{18}F]fluoride, as observed in our study. On the other hand, at the microscale, we previously concluded in the previous section that the reagents are a negligible source of ^{19}F-contamination. As more radioactivity is added, we thus expect the dominant source of [^{19}F]fluoride (cyclotron) to increase in proportion with [^{18}F]fluoride. Equation 1 becomes $A_m \approx A_m^{max}\,[^{18}F_C / (^{18}F_C + {}^{19}F_C)] \approx A_m^{max}\,(^{18}F_C/^{19}F_C)$. This expression is a constant for a given batch of the isotope, as we observed.

Effect of fluorinated materials

Radiolysis of fluorinated materials such as Teflon are known to lead to reduction in molar activity at the macroscale [37]. We investigated the possibility that the Teflon coating of the EWOD chips, in contact with reagents before and during the fluorination process, could adversely impact A_m in the microscale synthesis. Surprisingly, experiments assessing the impact of Teflon exposure to the initial [^{18}F]fluoride solution as a function of surface area, duration, and radioactivity showed negligible impact on the A_m of the resulting tracers (Supplementary Figure 1, Supplementary Discussion).

The above trends suggest that, in microfluidic ^{18}F-radiosynthesis, reagents and Teflon contact do not have an appreciable effect on A_m compared to cyclotron sources of ^{19}F-

Author Manuscript Author Manuscript Author Manuscript Author Manuscript

contamination. Microdroplet-based radiosynthesis therefore provides a route, under the radiochemist's control, for maximizing molar activity of PET tracers from a given batch of the radioisotope.

Effect of molar activity on *in vivo* imaging

While a few reports have compared the impact of low vs high molar activity in small animal imaging [20,47–49], this subject does not appear to have been extensively studied. In general, higher molar activity is expected to be important for imaging low density targets by reducing competition for binding sites with the non-radioactive form of the tracer. On the other hand, some tracers will benefit from lower A_m such as those with a substantial "sink" outside of the target tissue (e.g. non-specific binding or metabolism)[27]. In general, many factors could affect imaging and optimal molar activity may have to be evaluated experimentally for particular applications and having high A_m facilitates these evaluations.

We empirically studied the impact of molar activity on *in vivo* imaging of the saturable dopamine D2/D3 system with [^{18}F]fallypride. In two replicate experiments, a panel of mice were injected with the same amount of radioactivity, but each with a different A_m. Note that in this section, A_m values are corrected to the time of injection and not EOB. Static scans after 60 min uptake are shown in Figure 3. Substantial differences were observed in the images depending on A_m. In the first study (Figure 3a), $A_m \geq 0.49$ Ci/μmol [18 GBq/μmol] resulted in significant image contrast between striatum (region with high density of D2/D3 receptors) and cerebellum (where no binding is expected), but the striata remained undetectable at $A_m = 0.059$ Ci/μmol [2.2 GBq/μmol]. Similarly in the second study (Figure 3b), significant image contrast is seen at $A_m \geq 0.96$ Ci/μmol [36 GBq/μmol], whereas the striata was undetectable at $A_m = 0.009$ Ci/μmol [0.33 GBq/μmol]. These results, and calculated occupancies (see Supplementary Table 1, Supplementary Methods) are consistent with the report of Fischer *et al.* that this receptor system in mice is expected to starting showing significant (>10%) occupancy for injected amounts >4 nmol/kg [50].

Dynamic images revealed significant kinetic differences related to molar activity (see Supplementary Figures 2 and 3). For $A_m \geq 0.49$ Ci/μmol [18 GBq/μmol], [^{18}F]fallypride retention in the striatum (Supplementary Figures 2a, 3a) rapidly increased from the beginning of the scan until ~200 s. Retention remained nearly constant thereafter for $A_m \geq 0.96$ Ci/μmol [36 GBq/μmol], with signal intensity correlating with A_m. For $A_m \leq 0.49$ Ci/μmol [18 GBq/μmol], significant washout occurred after initial uptake, resulting in relatively low signal by the end of the 1 hr scan, with lower retention for lower A_m. For the lowest A_m in each study, the initial rapid uptake was not observed (didn't occur or was shorter than the frame duration). In the cerebellum, an initially high signal rapidly decreased (Supplementary Figures 2b, 3b), the decrease being faster for lower A_m. The striatum:cerebellum ratio increased over time and was generally higher for higher molar activity, though midrange A_m values (0.49 –2.0 Ci/μmol [18–74 GBq/μmol]) seemed to provide the greatest ratio (Supplementary Figures 2c, 3c). While additional studies involving more replicates and increased coverage of A_m values are needed to develop a better understanding of the influence of A_m, it is clear from these results that, at least for [^{18}F]fallypride, molar activity

Author Manuscript Author Manuscript Author Manuscript Author Manuscript

can have substantial impact on the quantitative analysis and qualitative interpretation of PET images.

Discussion

Our study showed that macroscale and microscale radiosynthesis had marked differences in the effect of several parameters on molar activity of ^{18}F-labeled PET tracers. The data suggest that the advantage of microscale synthesis is the minimization of ^{19}F-contamination in reagents. By reducing reaction volume by 2–3 orders of magnitude, sources of contamination in the synthesis became negligible in comparison to contamination already present in the initial [^{18}F]fluoride solution from the cyclotron. Microdroplet synthesis thus provides the radiochemist a tool for achieving the highest possible molar activity. The consistency of microscale A_m values over a wide range of conditions suggests that A_m likely matches $A_m^{isotope}$. Indeed, values are consistent with measurements over several years in our cyclotron facility suggesting $A_m^{isotope}$ is ~20 Ci/μmol [740 GBq/μmol]. Since other facilities have reported similar values [17], we expect comparable results could be achieved using [^{18}F]fluoride from other cyclotrons.

It should be appreciated that, in the microscale experiments presented here, high molar activity was achieved even using only very low starting radioactivity (e.g. 1 mCi [37 MBq]). Normally, the production of tracers with such high A_m requires starting with multiple Ci [e.g. 100–200 GBq] of radioactivity. The ability to work with orders of magnitude less radioactivity and still achieve high A_m has the important benefits of (i) greater safety, (ii) lower requirement for radiation shielding (e.g., enabling production to be performed with an L-block instead of a mini-cell or hot-cell), (iii) reduced radiation exposure during manual manipulations if needed, (iv) reduced radiation damage to equipment, tubing, etc., and (v) reduced radioisotope cost. Furthermore, if the tracer is intended for preclinical imaging, where especially high A_m may be critical [19], microscale synthesis makes it possible to produce only what is needed, as it is needed, rather than the conventional macroscale approach of a single high-radioactivity tracer production for the purpose of boosting A_m with much of the batch left unused. This is also an important concept for emerging technologies for benchtop production of PET tracers [51], where radiation shielding, and therefore total amount of radioactivity that can be safely handled, will be limited. In these cases, it might be impossible to produce sufficiently high A_m without the use of microvolume radiochemistry.

This ability to reliably synthesize tracers with high A_m provides important advantages in the screening and development of novel tracers, especially at early stages when very little may be known about toxicity, pharmacokinetics, target abundance, etc. Since the impact of A_m on qualitative and quantitative imaging can be significant, as was seen with [^{18}F]fallypride, it may be desirable to always err on the side of very high A_m to avoid potential pharmacologic response or target occupancy issues (which could lead to false negative results). Alternatively, it may be useful to be able to produce a small batch of a new tracer with very high A_m, aliquot several portions and adjust each to a different (lower) A_m by addition of non-radioactive tracer, and then studying the effect *in vivo* to determine the optimal range of molar activity for the intended application. High A_m also enables increases in throughput of

Author Manuscript Author Manuscript Author Manuscript Author Manuscript

animal experiments by enabling the batch of tracer to be used over a longer period of time and still have sufficient molar activity at the time of injection.

We suspect the ability of microscale radiosynthesis to achieve high molar activity is not limited to the model compounds chosen here, and can likely be generalized to most ^{18}F-labeled tracers [44] and potentially also to tracers labeled with other isotopes (e.g., radiometals). In addition to reducing isotopic contamination, microvolume radiochemistry may also provide a simple route to reduce the absolute amount of precursor used, while maintaining a high concentration of reagent during the radiolabeling reaction to ensure a fast reaction rate. This will improve A_m for isotopic exchange reactions [33] and apparent A_m for labeling of larger molecules such as proteins where labeled and unlabeled species cannot be separated during purification. Furthermore, reduction in precursor would likely enable simpler purification processes.

In summary, we showed that shrinking the volume scale of typical radiochemistry equipment from ~1 mL to the 1–10 μL range enabled the production of PET radiotracers with consistently high molar activity (~20 Ci/μmol [740 GBq/μmol]), independent of parameters such as the reaction volume and amount of starting radioactivity. Furthermore, these high A_m values could be obtained starting with very low amounts of radioactivity, providing a practical and safer means to prepare small amounts of high molar activity tracers. Automation of the overall microscale synthesis process, which is in progress in our laboratory and in collaboration with Sofie Biosciences [41], could enable more widespread access to the advantages of microscale radiosynthesis. Wider availability of high A_m PET tracers is critical in areas of neuroscience and drug development, and could streamline the process of developing novel tracers, or enable more thorough optimization of imaging protocols (i.e. considering A_m as a variable). In addition, it could enable the use of longer synthesis processes to produce PET tracers, enable transport of tracers across longer distances, or facilitate the development of benchtop radiosynthesizers for producing small batches of diverse tracers on demand.

Methods

Reagents

2,3-dimethyl-2-butanol (98%), anhydrous acetonitrile (MeCN; HPLC grade, >99.9%), anhydrous dimethylsulfoxide (DMSO; HPLC grade, 99.9%), hexane (HPLC grade, >97%), ethyl acetate (HPLC grade, >99.8%), ammonium formate ($HCOOHNH_4$) (HPLC grade, >99%), triethylamine (TEA; >99%), 1,4-dinitrobenzene (98%), 1-fluoro-4-nitrobenzene (99%), ethanol (EtOH; 200 proof), methanol (MeOH; HPLC grade, >99.9%), Fluorinert® FC40 and K_2CO_3 (>99%) were purchased from Sigma-Aldrich Chemical Co. (St. Louis, MO). 2,3-dimethoxy-5-[3-[[(4-methylphenyl)sulfoniyl]oxy]propyl]-N-[[1-(2-propenyl-2-pyrrolidinyl)methyl] (tosyl-Fallypride precursor) (>90%), Fallypride standard compound (>95%), tetrabutylammonium bicarbonate ($TBAHCO_3$) 0.075 M aq. solution stabilized with ethanol, and Cryptand-222 (K-222; >99%) were purchased from ABX Advanced Biochemical Compounds (Radeberg, Germany). Teflon® AF2400 solution (6%) for preparation of microfluidic chips was purchased from DuPont (USA). All chemicals were used without further purification.

Author Manuscript Author Manuscript Author Manuscript Author Manuscript

No-carrier-added [^{18}F]fluoride ion was obtained from the UCLA Biomedical Cyclotron Facility where it was produced by irradiation of 85% ^{18}O-enriched water with an 11 MeV proton beam using an RDS-112 cyclotron (Siemens Medical Solutions, Knoxville, TN). Typically, a ~1 Ci [37 GBq] bombardment was performed and the resulting [^{18}F]fluoride/[^{18}O]water solution was obtained in a volume of ~1.0 mL. The delivery time from the production site to our facility was sufficient to ensure any nitrogen-13 produced in the bombardment had decayed by the time of use.

Analytical methods

Radioactivity was determined using a calibrated ion chamber (CRC-25 PET, Capintec).

Fluorination efficiency (conversion efficiency) was analyzed via radio thin layer chromatography (radio-TLC). A sample was spotted onto a TLC plate (IB-F silica gel plates, BakerFlex). After developing in the mobile phase, the plate was dried and scanned by a radio-TLC scanner (MiniGITA star, Raytest USA, Inc, Wilmington, NC). Mobile phase for analysis of [^{18}F]Fallypride was 60:40 (v/v) MeCN:25 mM ammonium formate with 1%TEA, and the mobile phase for [^{18}F]FNB was 60:40 (v/v) MeCN:H_2O. R_f values for unreacted [^{18}F]fluoride, [^{18}F]Fallypride, and [^{18}F]FNB were 0.0, ~0.75, and ~0.80, respectively.

Analytical HPLC analysis for determination of purity and molar activity was performed on a Smartline HPLC system (Knauer, Germany), equipped with a degasser (Model 5050), pump (Model 1000), Phenomenex Luna reversed-phase C-18 column (250 × 4.6 mm) equipped with guard column (SecurityGuard C-18, Phenomenex, Torrance, CA), a variable wavelength UV detector (Model 2500) and a radiometric detector (Bioscan B-FC-4000, Bioscan Inc., Washington DC, USA). For [^{18}F]Fallypride samples, the mobile phase used was 60:40 (v/v) MeCN: 25 mM ammonium formate with 1% v/v TEA at a flow rate of 1.5 mL/min. The retention time of Fallypride was ~ 8.0 min. For [^{18}F]FNB, the mobile phase used was 55:45 (v/v) MeCN:H_2O at a flow rate of 1 mL/min. The retention time of [^{18}F]FNB was ~ 25 min.

Determination of molar activity

A 20 μL portion of the unknown sample was aspirated in a 50 μL glass syringe (Hamilton) and the radioactivity was measured via dose calibrator. The sample was injected into HPLC, and the radioactivity of the empty syringe was measured. The decay-corrected difference in measurements represents the actual amount of radioactivity injected into HPLC. For samples comprising crude reaction products, this amount of radioactivity also includes any impurities that may be present in the crude mixture (e.g. unreacted [^{18}F]fluoride and other ^{18}F-labeled species); therefore, the radioactivity amount was further corrected by multiplying by the radiochemical purity (RCP) of the desired species. Because of known losses of [^{18}F]fluoride in HPLC columns[52], the radiochemical purity was determined via a two-step process. (i) Radio-TLC analysis of the sample yielded a chromatogram with two peaks: one (R_f = 0.0) representing unreacted [^{18}F]fluoride, and the other (R_f = ~0.75 for Fallypride, R_f = ~0.8 for FNB) representing the radiofluorinated product (plus other potential fluorinated impurities). The area of the second peak divided by area of both peaks represents the fraction of non-

Author Manuscript Author Manuscript Author Manuscript Author Manuscript

fluoride species. (ii) From the radio-HPLC analysis, a chromatogram is obtained from the radiation detector, showing separation of the various non-fluoride radioactive species. The fraction of desired product is calculated by dividing the area under the peak matching the desired non-radioactive standard by the sum of areas of all other peaks (ignoring the underestimated fluoride peak). The RCP is the product of these two fractions. The injected radioactivity is then multiplied by the RCP to estimate the amount of the desired product ([^{18}F]Fallypride or [^{18}F]FNB) that was actually injected into the radio-HPLC.

From the UV detector chromatogram, the area under the curve (AUC) of the peak corresponding to the tracer is determined. Using the appropriate calibration curve, this value is converted to the number of moles of compound injected. Finally, the determined radioactivity value was divided by molar amount of the tracer to obtain the molar activity.

To avoid introducing A_m variations caused by different times of use of the radioactivity, which would confound the phenomena we were trying to study, all A_m values were decay-corrected to the end of bombardment (EOB). For imaging purposes, we recognize that one would generally be interested in the molar activity at the time of injection. Assuming the synthesis is started at EOB (to maximize A_m and the available amount of radioactivity), then A_m at the time of injection would typically be 43% lower than the decay-corrected values we report (estimating synthesis and formulation time of ~90 min).

To build the calibration curves (Supplementary Figure 4), stock solutions of Fallypride and FNB reference standards were injected into HPLC, resulting in chromatograms with a single peak. The amount injected was varied by using different injection volumes. The AUC of each peak was determined, and the AUCs were plotted as a function of injected amount of each compound. A linear least squares fit was then performed for each compound (R^2 = 0.9906 for Fallypride and R^2 = 0.9986 for FNB). The range of concentrations was chosen to cover the expected range of masses in samples.

Theoretically, chlorination of the precursor is also possible by chloride ions that may be present as contamination in the initial [^{18}F]fluoride solution originating from the cyclotron or might be present in reagents. To ensure that UV peaks represent only the fluorinated form, we compared the retention times of the standard solutions of the fluoro- and chloro-derivatives (Supplementary Figure 5). These forms will well-separated, ruling out the possibility that the chloro-derivatives could affect the molar activity measurements.

Microscale radiosynthesis platform

Microscale radiosynthesis was carried out in droplets on model EWOD chips consisting of Teflon AF-coated glass slides (Figure 2). These simplified chips are significantly less expensive than EWOD chips, but have similar thermal properties and identical materials in contact with the reaction mixture. Fabrication of chips was similar to previously reported methods [40]. The chips were made from glass pieces (25 mm x 25 mm) cut from standard microscope slides (Fisherbrand Plain Glass Microscope Slides). After cleaning with MeOH, acetone, and DI water, the glass pieces were spin-coated with a 1% Teflon® AF2400 solution (prepared by diluting the 6% solution with Fluorinert® FC40). The coating protocol consisted of three steps: 5s at 500 rpm (100 rpm/s ramping rate), 30s at 1000 rpm (100 rpm/s

Author Manuscript Author Manuscript Author Manuscript Author Manuscript

ramping rate), and then 0 rpm (500 rpm/s ramping rate). Subsequently, Teflon-coated glass slides were placed in an open Pyrex® Petri dish, and underwent baking on a hotplate at 150, 180 and 350 °C for 10, 10, and 60 min, respectively, to remove solvent and anneal the Teflon layer.

To control temperature, the chip was affixed on top of a small aluminum heating block (1 × 1 × 1 cm) containing a thermistor for temperature measurement. The heating block was in turn was placed on top of a thermoelectric (Peltier) heating/cooling element. Temperature was maintained using a thermoelectric controller (5R7–001, McShane Inc., Medina, OH, USA). Thermal paste (OmegaTherm 201, Omega Engineering, Inc., Norwalk, CT, USA) was applied between components to ensure good thermal contact. Reagents were loaded onto the chip via micropipette.

Microscale radiosynthesis of [^{18}F]Fallypride

The microscale synthesis of [^{18}F]Fallypride was adapted from our previous reports [43,45]. A [^{18}F]fluoride/base stock solution was prepared by mixing 0.075M $TBAHCO_3$ (5 μL) with [^{18}F]fluoride/[^{18}O]H_2O (100 μL; ~100 mCi [3.7 GBq]), corresponding to an initial radioactivity concentration of ~1.0 mCi/μL [37 MBq/μL]. A precursor stock solution was prepared by dissolving tosyl-Fallypride (4 mg) in 1:1 v/v MeCN/thexyl alcohol (100 μL).

A droplet of the [^{18}F]fluoride/base stock solution (8 μL) and a droplet of MeCN (8μL) were first deposited on a new chip. To achieve a total radioactivity of ~20 mCi [0.74 GBq], additional [^{18}F]fluoride/[^{18}O]water (12 μL) and MeCN (12 μL) were added. The chip was heated to 105°C (actual ramp time ~140 s) to evaporate the solvent, leaving a dried residue of the [^{18}F]TBAF complex. Residual water was removed by adding another droplet of MeCN (8 μL) and evaporating at 105°C for 1 min. Note that the dried residue covers an area much smaller than the original droplet size. A droplet of precursor solution (4 μL) was added to the residue site, and the reaction droplet was then sandwiched by placing a separate Teflon-glass plate as a “cover plate” on top of the droplet. The gap height was set to ~150 μm by using small pieces of double-sided Scotch 3M tape spacers attached to the edges of the second glass plate. The fluorination reaction was performed by heating to 105°C for 7 min. To collect the crude product for analysis, the top chip was removed and a droplet of MeOH (20 μL) was added to each chip, briefly mixed, and collected with a pipette. This process was repeated an additional time, resulting in a total collected volume of ~80 μL.

When used for imaging, the crude [^{18}F]Fallypride was purified using the analytical-scale HPLC method described above, except with flow rate of 1 mL/min (giving retention time of ~12 min). The collected eluate was subsequently evaporated in a V-vial using an oil bath (110 °C), redissolved in a 3% v/v EtOH:saline mixture (1 mL) and passed through 0.22 μm sterilizing filter (Anotop® 10 Plus, Whatman) into a sterile empty vial. The final activity in the product vial was ~10 mCi [0.37 GBq].

Microscale radiosynthesis of [^{18}F]FNB

The microscale synthesis of [^{18}F]FNB was performed similarly by adapting the macroscale conditions reported by Collins *et al.* [53]. A base stock solution was first prepared by dissolving K_2CO_3 (2.5 mg) and K-222 (30 mg) in water (350 μL). A 50 μL aliquot was

Author Manuscript Author Manuscript Author Manuscript Author Manuscript

mixed with 50 μL of [^{18}F]fluoride/[^{18}O]H_2O (~50 mCi [1.9 GBq]) to prepare the [^{18}F]fluoride/base stock solution, corresponding to a radioactivity concentration of ~0.5 mCi/μL [~19MBq/μL]. A precursor stock solution was prepared by mixing 1,4-dinitrobenzene (2.5 mg) in 145 μL of DMSO.

A droplet of the [^{18}F]fluoride/base solution (8 μL) and a droplet of MeCN (8 μL) were added onto a new chip, followed by additional droplets of [^{18}F]fluoride/[^{18}O]water (16 μL) and MeCN (16 μL) to yield a total radioactivity of ~20 mCi [0.74 GBq]. The chip was heated to 105°C to evaporate the solvent. After cooling, an additional droplet of MeCN (8 μL) was added and evaporated at 105°C for 1 min to azeotropically dry the [^{18}F]KF/K-222 complex. The precursor solution droplet (4 μL) was then added and a cover chip installed. The chip was heated to 130°C (actual ramp time ~210 s) for 5 min to perform the fluorination reaction. After cooling to 25 °C (actual ramp time ~170 s), the crude product was collected in MeOH in the same fashion as for [^{18}F]Fallypride.

Macroscale radiosynthesis apparatus

Macroscale radiosyntheses were performed using the ELIXYS automated radiosynthesizer (Sofie Biosciences, Inc., Culver City, CA, USA) [54,55].

Macroscale radiosynthesis of [^{18}F]Fallypride

The macroscale synthesis of [^{18}F]Fallypride was adapted from our previous report [55]. A base stock solution was prepared by mixing 0.075M $TBAHCO_3$ (600 μL) and MeCN (1 mL). A precursor stock solution was prepared by dissolving tosyl-fallypride (4 mg) in 1:1 v/v MeCH:thexyl alcohol (0.5 mL).

First, the reactor vial was loaded with a solution of [^{18}F]fluoride/[^{18}O]H_2O (20 μL; ~20 mCi [0.74 GBq]) and base stock solution (1.6 mL), and subsequently dried at 110°C until almost dry (2.5 min). Anhydrous MeCN (1 mL) was then added to reaction vial to azeotropically remove water from the solution by heating at 110°C until complete dryness (1.5 min). This step was repeated an additional time to ensure sufficient removal of water. Next, precursor solution (0.5 mL) was added into reactor vial containing the dried [^{18}F]TBAF complex. The fluorination reaction was performed at 110°C for 7 min, and the resulting crude mixture was analyzed.

Macroscale radiosynthesis of [^{18}F]FNB

The macroscale synthesis of [^{18}F]FNB was adapted from the procedure of Collins *et al.* [53]. Base stock solution was prepared by dissolving K_2CO_3 (12 mg) in H_2O (1200 μL). Cryptand stock solution was prepared by dissolving K-222 (120 mg) in MeCN (5400 μL). A precursor stock solution was prepared by mixing 1,4-dinitrobenzene (2 mg) in DMSO (1 mL).

First, the reactor vial was loaded with solutions of [^{18}F]fluoride/[^{18}O]H_2O (20 μL; ~20 mCi [0.74 GBq]), base stock solution (100 μL), cryptand stock solution (900 μL), and acetonitrile (1 mL). Drying was performed in an identical fashion as for [^{18}F]Fallypride. Next, precursor stock solution (1 mL) was added into reactor vial containing the dried [^{18}F]KF/K-222

Author Manuscript Author Manuscript Author Manuscript Author Manuscript

complex. The fluorination reaction was performed at 130°C for 7 min, and then the reactor was cooled for analysis of the crude product.

Molar activity comparisons

The effect of several different synthesis factors on A_m was investigated via a systematic series of experiments. Sets of experiments were always performed from a single batch of [^{18}F]fluoride/[^{18}O]water to eliminate potential day-to-day variation (e.g. of $A_m^{isotope}$) as a variable. In addition, all the chips used throughout the whole day were taken from the same fabrication batch, and reagents and solvents used were taken from the same product batch.

Note that processing of [^{18}F]fluoride via an anion exchange cartridge (e.g. quaternary methylammonium, QMA) was not performed in these studies, as the ^{19}F-contamination introduced in typical preconditioning processes [39] could confound the measurements. Detailed investigation of this step and optimization for high A_m will be performed in the future.

Effect of reaction volume on molar activity

To understand the influence of reagent amounts on [^{19}F]fluoride contamination, experiments were performed in which the volume of [^{18}F]fluoride/[^{18}O]H_2O was held constant, while the volume of reagent stock solutions (base, phase transfer catalyst, precursor) were varied proportionally. The influence of reaction volume on A_m was studied at both the microscale ([^{18}F]Fallypride and [^{18}F]FNB) and macroscale ([^{18}F]FNB). In the macroscale case (Figure 3a), identical amounts of [^{18}F]fluoride/[^{18}O]water (30 μL; ~30 mCi [1.1 GBq]) were loaded into each of 4 empty reaction vials. The amounts of all other reagents were scaled proportionally to ensure consistent concentrations and reagent ratios (see Supplementary Table 2). Different volumes of base / phase transfer catalyst stock solutions were added to each vial during [^{18}F]fluoride dyring, and corresponding volumes of precursor stock solution were added to each vial during the fluorination reaction. Reactions were performed in a back-to-back fashion in the ELIXYS radiosynthesizer using multiple reactor positions, and multiple reagent delivery positions for each reactor. A_m was compared for the different reactions. The set of 4 reactions was repeated 3 times (on different days). The microscale syntheses were performed in an analogous fashion (Figure 3c) at slightly smaller radioactivity scale (~20 mCi [0.74 GBq]). Different amounts [^{18}F]fluoride/base mixture, MeCN, and [^{18}F]fluoride/[^{18}O]water (see Supplementary Table 3) were loaded onto each of 4 chips to achieve an analogous comparison (i.e. identical amounts of [^{18}F]fluoride/[^{18}O]H_2O but varied amount of other reagents), and the syntheses was carried out at described above. A_m of the crude reaction mixtures from different chips were compared. The set of 4 reactions was repeated 3 times (on different days) for each of the model compounds.

Effect of starting radioactivity on molar activity

The effect of starting radioactivity on A_m was explored at both the macroscale and microscale for both model compounds. For the macroscale case (Figure 3b), different volumes of [^{18}F]fluoride/[^{18}O]water were initially loaded into the reaction vials to achieve different starting radioactivity. [^{18}F]Fallypride synthesis was carried out as described above, and [^{18}F]FNB synthesis was carried out as described above except all reagent volumes were

Author Manuscript Author Manuscript Author Manuscript Author Manuscript

reduced 2x (i.e. to match 500 μL fluorination volume). For the microscale experiments (Figure 3d), synthesis of the two compounds was performed as described above (i.e. with 4 μL fluorination reaction volume), except varied volumes of additional [^{18}F]fluoride/[^{18}O]H_2O were added after the 8 μL of [^{18}F]fluoride/base solution to achieve different starting radioactivities. Note that when the total volume was >200 μL, the capacity of the chip was exceeded, and it was necessary to load a portion at a time (up to 200 μL) and dry it, before adding the next portion.

Effects of Teflon surface on molar activity

Since it is known that radiolysis of bulk Teflon can introduce [^{19}F]fluoride ion into the reaction mixture in proportion to the time of exposure, surface area of exposure, and amount of radioactivity [37], we also performed several experiments to evaluate if there is any influence of the Teflon coating on molar activity of a probe synthesized using the microchip (see Supplementary Methods).

In vivo imaging and analysis

Beginning with a high A_m production of [^{18}F]Fallypride using a microfluidic chip, four formulations with different A_m (at time of injection) were prepared by relying both on radioactive decay and spiking with non-radioactive standard ([^{19}F]Fallypride). A_m of each formulation was separately measured via analytical radio-HPLC just prior to injection. Static and dynamic imaging was performed to determine the effects of A_m on imaging.

All *in vivo* imaging studies were conducted in accordance with UCLA Animal Research Committee approved protocols and guidelines. Healthy female BALB/c mice (8 weeks old) were anesthetized with 2% isoflurane in oxygen, catheterized via tail vein, and injected with ~100 μCi [~3.7 MBq] [^{18}F]Fallypride via catheter. Mice underwent either 10-min static PET scans after a 60 min uptake period under anesthesia or 70-min dynamic PET scans (Inveon microPET, Siemens Medical Solutions USA Inc.). Images were processed with 3D histogramming and reconstruction with a zoom factor of 2.1 using 3D-OSEM with 2 iterations followed by MAP with 18 iterations. All PET procedures were followed with CT scans (CrumpCAT microCT [56]) for anatomical co-registration. PET/CT images were analyzed using AMIDE version 1.0.5 [57]. Regions of interest (ROIs) were drawn for the left striatum, right striatum, and cerebellum to calculate the ratio of specific (striatal) to non-specific (cerebellum) [^{18}F]Fallypride binding.

Supplementary Material

Refer to Web version on PubMed Central for supplementary material.

Acknolwedgments

The authors thank Dr. Saman Sadeghi, Dr. Umesh Gangadharmath, and the staff of the UCLA Biomedical Cyclotron Facility for generously providing [^{18}F]fluoride for these studies, and Dr. Sung-Cheng (Henry) Huang for valuable discussions about image analysis. This work was supported in part by the National Institute of Biomedical Imaging and Bioengineering (R21 EB015540, T32 EB002101), the National Institute on Aging (R21 AG049918), the National Cancer Institute (U54 CA151819A, i.e. the Caltech/UCLA Nanosystems Biology Cancer Center), the Department of Energy Office of Biological and Environmental Research (DE-SC0005056), and the UCLA Foundation from a donation made by Ralph and Marjorie Crump for the Crump Institute for Molecular imaging.

Author Manuscript Author Manuscript Author Manuscript Author Manuscript

The UCLA Crump Institute's Preclinical Imaging Technology Center is supported in part by the NIH In Vivo Cellular and Molecular Imaging Centers Grant (P50 CA086306), NIH Cancer Center Support Grant (P30 CA016042), and NIH SPORE Grant (P50 CA092131).

References

1. Vallabhajosula S, Solnes L & Vallabhajosula B A Broad Overview of Positron Emission Tomography Radiopharmaceuticals and Clinical Applications: What Is New? Semin. Nucl. Med 41, 246–264 (2011). [PubMed: 21624560]
2. Ametamey SM, Honer M & Schubiger PA Molecular Imaging with PET. Chem. Rev 108, 1501–1516 (2008). [PubMed: 18426240]
3. Hargreaves R et al. Optimizing Central Nervous System Drug Development Using Molecular Imaging. Clin. Pharmacol. Ther 98, 47–60 (2015). [PubMed: 25869938]
4. Willmann JK, van Bruggen N, Dinkelborg LM & Gambhir SS Molecular imaging in drug development. Nat. Rev. Drug Discov 7, 591–607 (2008). [PubMed: 18591980]
5. Matthews PM, Rabiner EA, Passchier J & Gunn RN Positron emission tomography molecular imaging for drug development. Br. J. Clin. Pharmacol 73, 175–186 (2012). [PubMed: 21838787]
6. Zhu L, Ploessl K & Kung HF PET/SPECT imaging agents for neurodegenerative diseases. Chem. Soc. Rev 43, 6683–6691 (2014). [PubMed: 24676152]
7. Honer M, Gobbi L, Martarello L & Comley RA Radioligand development for molecular imaging of the central nervous system with positron emission tomography. Drug Discov. Today 19, 1936–1944 (2014). [PubMed: 25173703]
8. Phelps ME Molecular Imaging with Positron Emission Tomography. Annu. Rev. Nucl. Part. Sci 52, 303–338 (2002).
9. Phelps ME Positron emission tomography provides molecular imaging of biological processes. Proc. Natl. Acad. Sci 97, 9226–9233 (2000). [PubMed: 10922074]
10. Radiosynthesis Database of PET Probes (RaDaP). Available at: http://www.nirs.qst.go.jp/research/division/mic/db2/. (Accessed: 8th May 2017)
11. Alauddin MM Positron emission tomography (PET) imaging with 18F-based radiotracers. Am. J. Nucl. Med. Mol. Imaging 2, 55–76 (2012). [PubMed: 23133802]
12. Shiue Chyng-Yann, Fowler Joanna S., Wolf Alfred P., Watanabe Masazumi & Arnett Carroll D.. Synthesis and Specific Activity Determinations of No-Carrier-Added Fluorine-18-Labeled Neuroleptic Drugs. J. Nucl. Med 26, 181–186 (1985). [PubMed: 2857191]
13. Gmez-Vallejo V, Gaja V, Koziorowski J & Llop J Specific Activity of 11C-Labelled Radiotracers: A Big Challenge for PET Chemists. in Positron Emission Tomography - Current Clinical and Research Aspects (ed. Hsieh C-H) (InTech, 2012).
14. Eckelman WC, Bonardi M & Volkert WA True radiotracers: are we approaching theoretical specific activity with Tc-99m and I-123? Nucl. Med. Biol 35, 523–527 (2008). [PubMed: 18589295]
15. Cai L, Lu S & Pike VW Chemistry with [18F]Fluoride Ion. Eur. J. Org. Chem 2008, 2853–2873 (2008).
16. Liu Z et al. Stoichiometric Leverage: Rapid 18F-Aryltrifluoroborate Radiosynthesis at High Specific Activity for Click Conjugation. Angew. Chem. Int. Ed 52, 2303–2307 (2013).
17. Liu Z et al. Kit-like 18F-labeling of RGD-19F-Arytrifluroborate in high yield and at extraordinarily high specific activity with preliminary in vivo tumor imaging. Nucl. Med. Biol 40, 841–849 (2013). [PubMed: 23810487]
18. Innis RB et al. Consensus Nomenclature for in vivo Imaging of Reversibly Binding Radioligands. J. Cereb. Blood Flow Metab 27, 1533–1539 (2007). [PubMed: 17519979]
19. Hume SP, Gunn RN & Jones T Pharmacological constraints associated with positron emission tomographic scanning of small laboratory animals. Eur. J. Nucl. Med. Mol. Imaging 25, 173–176 (1998).
20. Jagoda EM, Vaquero JJ, Seidel J, Green MV & Eckelman WC Experiment assessment of mass effects in the rat: implications for small animal PET imaging. Nucl. Med. Biol 31, 771–779 (2004). [PubMed: 15246368]

Author Manuscript Author Manuscript Author Manuscript Author Manuscript

21. Madsen K, Marner L, Haahr M, Gillings N & Knudsen GM Mass dose effects and in vivo affinity in brain PET receptor studies — a study of cerebral 5-HT4 receptor binding with [11C]SB207145. Nucl. Med. Biol 38, 1085–1091 (2011). [PubMed: 21831646]
22. Bergström M, Grahnén A & Långström B Positron emission tomography microdosing: a new concept with application in tracer and early clinical drug development. Eur. J. Clin. Pharmacol 59, 357–366 (2003). [PubMed: 12937873]
23. Lappin G & Garner RC Big physics, small doses: the use of AMS and PET in human microdosing of development drugs. Nat. Rev. Drug Discov 2, 233–240 (2003). [PubMed: 12612650]
24. Rani Pu. & Naidu MU. Phase 0 - Microdosing strategy in clinical trials. Indian J. Pharmacol 40, 240–242 (2008). [PubMed: 21279177]
25. Agdeppa E & Spilker M A Review of Imaging Agent Development. AAPS J. 11, 286–299 (2009). [PubMed: 19415506]
26. Liu Z et al. Rapid, one-step, high yielding 18F-labeling of an aryltrifluoroborate bioconjugate by isotope exchange at very high specific activity. J. Label. Compd. Radiopharm 55, 491–496 (2012).
27. Kung M-P & Kung HF Mass effect of injected dose in small rodent imaging by SPECT and PET. Nucl. Med. Biol 32, 673–678 (2005). [PubMed: 16243641]
28. Lapi SE & Welch MJ A historical perspective on the specific activity of radiopharmaceuticals: What have we learned in the 35 years of the ISRC? Nucl. Med. Biol 40, 314–320 (2013). [PubMed: 23357081]
29. Libert LC et al. Production at the Curie Level of No-Carrier-Added 6–18F-Fluoro-l-Dopa. J. Nucl. Med 54, 1154–1161 (2013). [PubMed: 23658219]
30. Lemaire C et al. Automated production at the curie level of no-carrier-added 6-[18F]fluoro- l-dopa and 2-[18F]fluoro- l-tyrosine on a FASTlab synthesizer. J. Label. Compd. Radiopharm 58, 281–290 (2015).
31. Ravert HT et al. An improved synthesis of the radiolabeled prostate-specific membrane antigen inhibitor, [18F]DCFPyL. J. Label. Compd. Radiopharm 59, 439–450 (2016).
32. Scott PJH et al. Studies into radiolytic decomposition of fluorine-18 labeled radiopharmaceuticals for positron emission tomography. Appl. Radiat. Isot 67, 88–94 (2009). [PubMed: 18951032]
33. Bernard-Gauthier V et al. From Unorthodox to Established: The Current Status of 18F-Trifluoroborate- and 18F-SiFA-Based Radiopharmaceuticals in PET Nuclear Imaging. Bioconjug. Chem 27, 267–279 (2016). [PubMed: 26566577]
34. Solin O, Bergman J, Haaparanta M & Reissell A Production of 18F from water targets. Specific radioactivity and anionic contaminants. Int. J. Rad. Appl. Instrum. [A] 39, 1065–1071 (1988).
35. Füchtner F, Preusche S, Mäding P, Zessin J & Steinbach J Factors affecting the specific activity of [18F]fluoride from a [18O]water target. Nukl. Nucl. Med 47, 116–119 (2008).
36. Satyamurthy N, Amarasekera B, Alvord CW, Barrio JR & Phelps ME Tantalum [18O]Water Target for the Production of [18F]Fluoride with High Reactivity for the Preparation of 2-Deoxy-2-[18F]Fluoro-D-Glucose. Mol. Imaging Biol 4, 65–70 (2002). [PubMed: 14538049]
37. Berridge MS, Apana SM & Hersh JM Teflon radiolysis as the major source of carrier in fluorine-18. J. Label. Compd. Radiopharm 52, 543–548 (2009).
38. Link JM, Shoner SC & Krohn KA Sources of carrier F-19 in F-18 fluoride. in AIP Conference Proceedings 1509, 61–65 (AIP Publishing, 2012).
39. Lu S, Giamis AM & Pike VW Synthesis of [18F]fallypride in a micro-reactor: rapid optimization and multiple-production in small doses for micro-PET studies. Curr. Radiopharm 2, 1–13 (2009).
40. Keng PY et al. Micro-chemical synthesis of molecular probes on an electronic microfluidic device. Proc. Natl. Acad. Sci 109, 690–695 (2012). [PubMed: 22210110]
41. Keng PY & van Dam RM Digital Microfluidics: A New Paradigm for Radiochemistry. Mol. Imaging 14, 579–594 (2015).
42. Elizarov AM et al. Design and Optimization of Coin-Shaped Microreactor Chips for PET Radiopharmaceutical Synthesis. J Nucl Med 51, 282–287 (2010). [PubMed: 20124050]
43. Javed MR et al. High yield and high specific activity synthesis of [18F]fallypride in a batch microfluidic reactor for micro-PET imaging. Chem. Commun 50, 1192–1194 (2014).

Author Manuscript Author Manuscript Author Manuscript Author Manuscript

44. Javed MR et al. Efficient Radiosynthesis of 3′-Deoxy-3′−18F-Fluorothymidine Using Electrowetting-on-Dielectric Digital Microfluidic Chip. J. Nucl. Med 55, 321–328 (2014). [PubMed: 24365651]
45. Chen S et al. Radiolabelling diverse positron emission tomography (PET) tracers using a single digital microfluidic reactor chip. Lab. Chip 14, 902–910 (2014). [PubMed: 24352530]
46. Keng PY, Sergeev M & van Dam RM Advantages of Radiochemistry in Microliter Volumes. in Perspectives on Nuclear Medicine for Molecular Diagnosis and Integrated Therapy (eds. Kuge Y, Shiga T & Tamaki N) 93–111 (Springer Japan, 2016). doi:10.1007/978-4-431-55894-1_7
47. Rominger A et al. Validation of the Octamouse for Simultaneous 18F-Fallypride Small-Animal PET Recordings from 8 Mice. J. Nucl. Med 51, 1576–1583 (2010). [PubMed: 20847158]
48. Honer M, Brühlmeier M, Missimer J, Schubiger AP & Ametamey SM Dynamic Imaging of Striatal D2 Receptors in Mice Using Quad-HIDAC PET. J. Nucl. Med 45, 464–470 (2004). [PubMed: 15001689]
49. Kuik W-J et al. In Vivo Biodistribution of No-Carrier-Added 6–18F-Fluoro-3,4-Dihydroxy-L-Phenylalanine (18F-DOPA), Produced by a New Nucleophilic Substitution Approach, Compared with Carrier-Added 18F-DOPA, Prepared by Conventional Electrophilic Substitution. J. Nucl. Med 56, 106–112 (2015). [PubMed: 25500826]
50. Fischer K et al. Noninvasive Nuclear Imaging Enables the In Vivo Quantification of Striatal Dopamine Receptor Expression and Raclopride Affinity in Mice. J. Nucl. Med 52, 1133–1141 (2011). [PubMed: 21680681]
51. Keng PY, Esterby M & van Dam RM Emerging Technologies for Decentralized Production of PET Tracers. in Positron Emission Tomography - Current Clinical and Research Aspects (ed. Hsieh C-H) 153–182 (InTech, 2012).
52. Ory D et al. Retention of [18F]fluoride on reversed phase HPLC columns. J. Pharm. Biomed. Anal. 111, 209–214 (2015). [PubMed: 25898315]
53. Collins M, Lasne M-C & Barré L Rapid synthesis of N,N′-disubstituted piperazines. Application to the preparation of No carrier added 1-(4-[18F]fluorophenyl)piperazine and of an [18F]-selective ligand of serotoninergic receptors (5HT2 antagonist). J. Chem. Soc. [Perkin 1] 3185–3188 (1992). doi:10.1039/P19920003185
54. Lazari M et al. ELIXYS - a fully automated, three-reactor high-pressure radiosynthesizer for development and routine production of diverse PET tracers. EJNMMI Res. 3, 52 (2013). [PubMed: 23849185]
55. Lazari M et al. Fully Automated Production of Diverse 18F-Labeled PET Tracers on the ELIXYS Multireactor Radiosynthesizer Without Hardware Modification. J. Nucl. Med. Technol 42, 203–210 (2014). [PubMed: 25033883]
56. Taschereau R, Vu NT & Chatziioannou AF Calibration and data standardization of a prototype bench-top preclinical CT. in 2014 IEEE Nuclear Science Symposium and Medical Imaging Conference (NSS/MIC) 1–2 (2014). doi:10.1109/NSSMIC.2014.7430845
57. Loening AM & Gambhir SS AMIDE: a free software tool for multimodality medical image analysis. Mol. Imaging 2, 131–137 (2003). [PubMed: 14649056]

Author Manuscript Author Manuscript Author Manuscript Author Manuscript

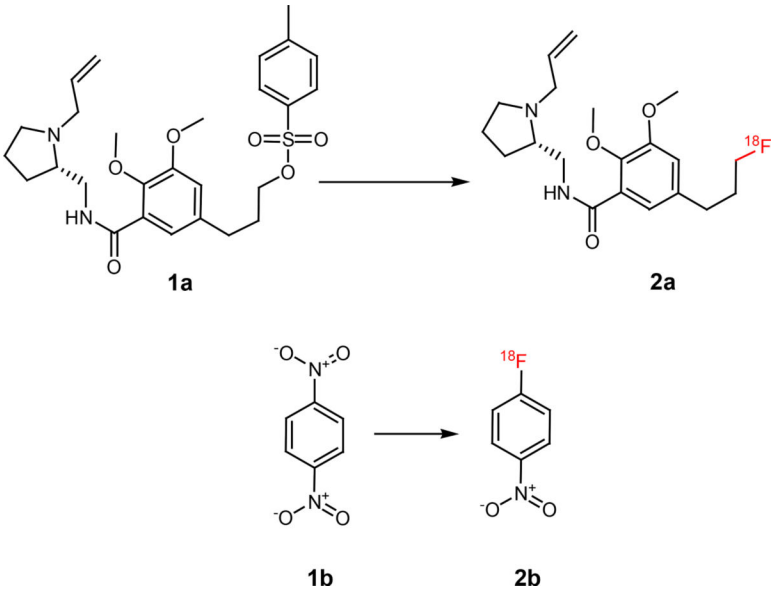

Figure 1: Model radiosyntheses

Reaction schemes for the radiosyntheses of [^{18}F]fallypride (**2a**) and [^{18}F]FNB (**2b**).

Author Manuscript Author Manuscript Author Manuscript Author Manuscript

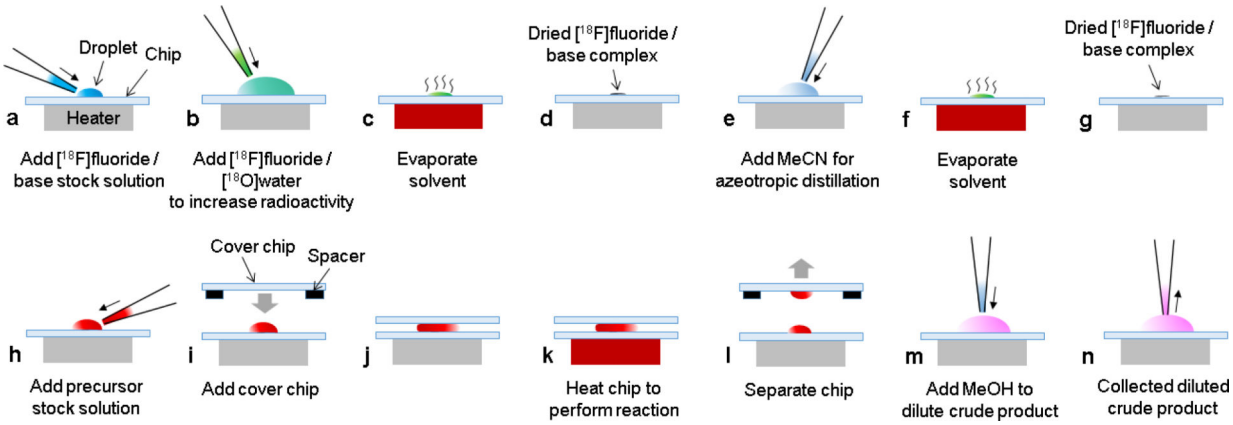

Figure 2: Schematic of microdroplet-based radiosynthesis process

(a) A fixed volume of [^{18}F]fluoride/base stock solution is added to the chip. (b) Additional [^{18}F]fluoride/[^{18}O]water (without base) is added to the chip to scale the amount of radioactivity. (c-d) The solvent is evaporated, leaving a dried residue. (e) MeCN is added. (f-g) Azeotropic distillation is performed to remove residual water and leave a dried residue of the [^{18}F]fluoride/base complex. (h) A fixed volume of the precursor stock solution is added, and the chip is covered (i-j). (k) The chip is heated to perform the reaction. (l) The chip is separated, and MeOH is added (m) to dilute the crude product. (n) The diluted product is removed from the chip. Steps m-n are repeated for the cover chip as well.

Author Manuscript Author Manuscript Author Manuscript Author Manuscript

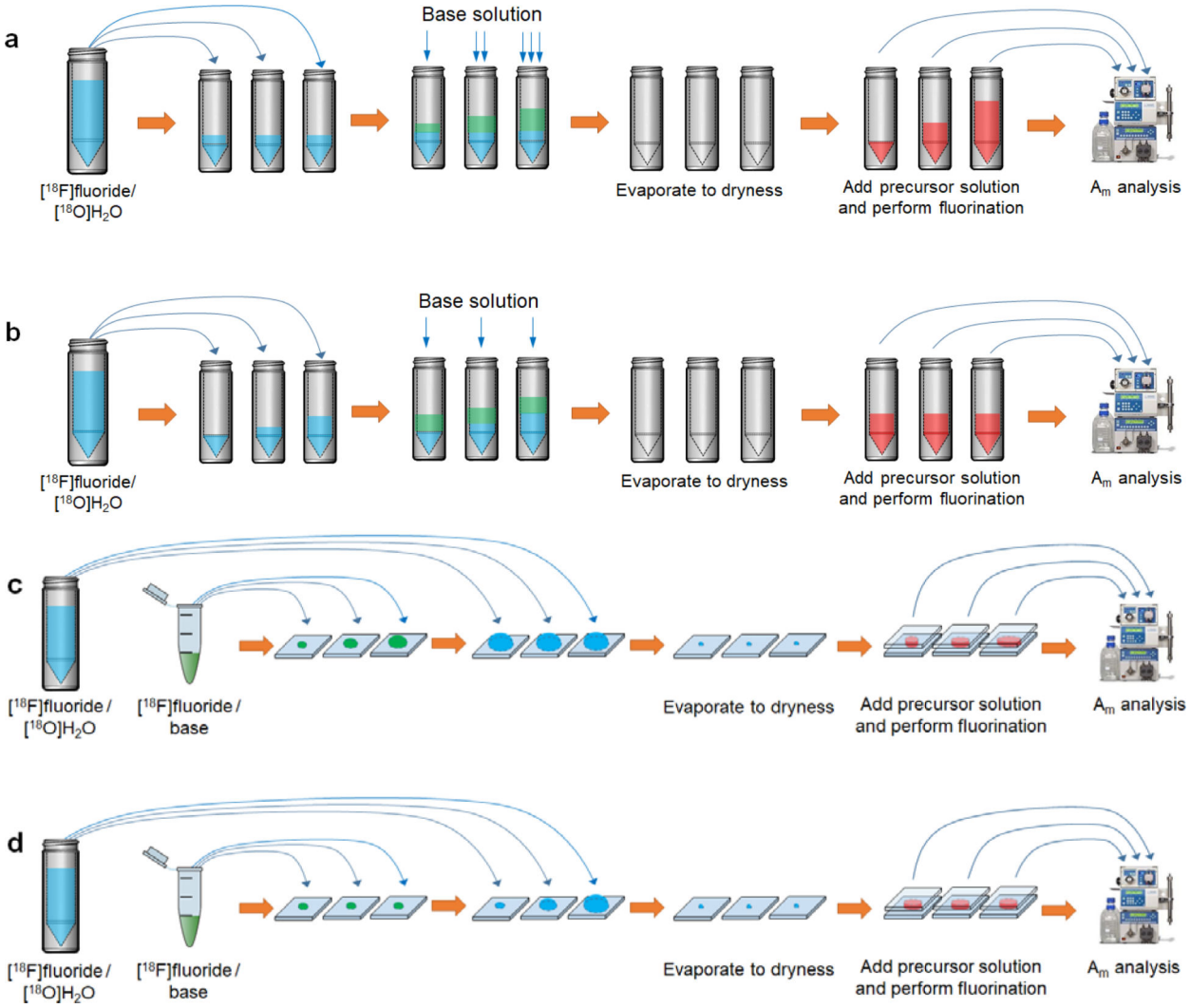

Figure 3: Experimental design for assessing the influence of variables on molar activity in macroscale and microscale radiosyntheses

(a) Effect of reagent volume (macroscale). Equal aliquots of [^{18}F]fluoride/[^{18}O]H_2O are added to reaction vials (to give equal starting radioactivity) followed by varying amounts of base solution. After evaporation to dryness, varying amounts of precursor (in proportion to base solution) are added and fluorination is performed. (b) Effect of starting radioactivity (macroscale). Varying amounts of [^{18}F]fluoride/[^{18}O]H_2O are added to reaction vials (to give varying starting radioactivity) followed by equal amounts of base solution. After drying, equal amounts of precursor solution are added and fluorination is performed. (c) Effect of reaction droplet volume (microscale). Different combinations of [^{18}F]fluoride/base solution and [^{18}F]fluoride/[^{18}O]H_2O solution are added to chips such that starting radioactivity is matched but the amount of base varies. Following drying, varying amounts of precursor solution are added (in proportion to base) and fluorination is performed. (d) Effect of starting radioactivity (microscale). Equal amounts of [^{18}F]fluoride/base and varying amounts of [^{18}F]fluoride/[^{18}O]H_2O are added to chips such that starting

radioactivity varies but amount of base is identical. Evaporation is performed and equal amounts of precursor solution are then added and fluorination is performed.

Author Manuscript Author Manuscript Author Manuscript Author Manuscript

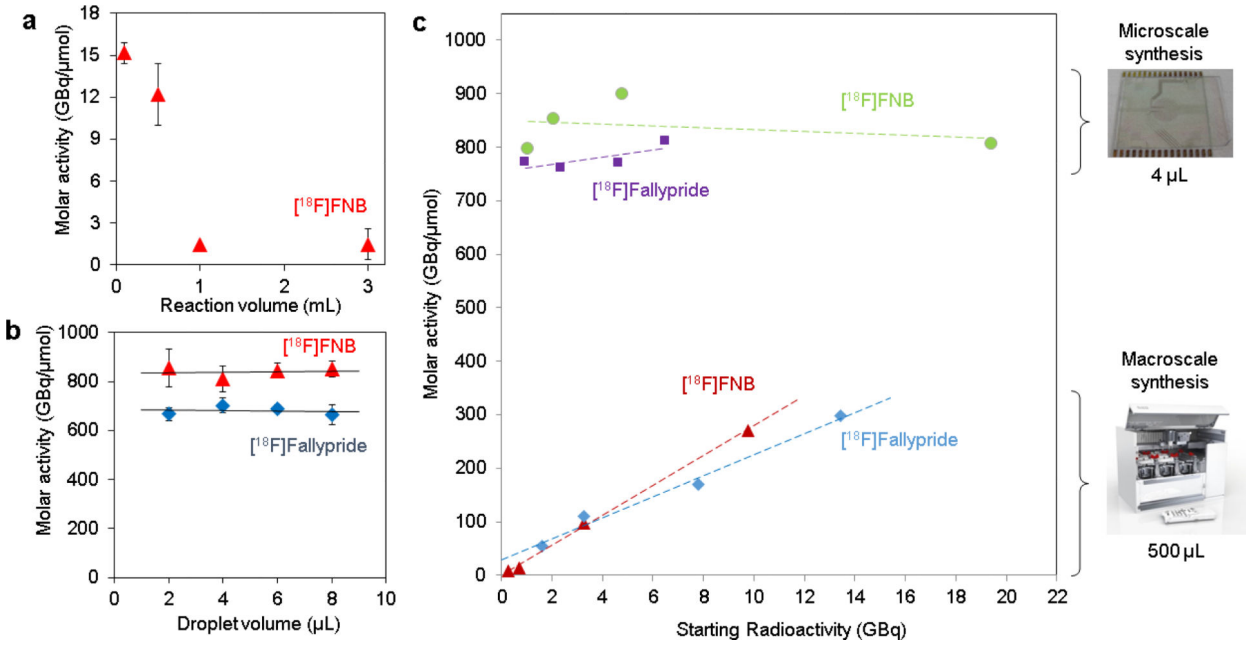

Figure 4: Comparison of parameter influence on molar activity at different synthesis scales.

Comparison of molar activity values as a function of reaction volumes in the (a) macroscale and (b) microscale. Data points represent the average obtained across 3 days of experiments; the error bars are standard deviations. (c) Molar activity of [^{18}F]FNB and [^{18}F]fallypride for different starting activity levels in microscale and macroscale syntheses. This set of experiments was performed n=1 time. All molar activity values are corrected to EOB.

Author Manuscript Author Manuscript Author Manuscript Author Manuscript

Author Manuscript Author Manuscript Author Manuscript Author Manuscript

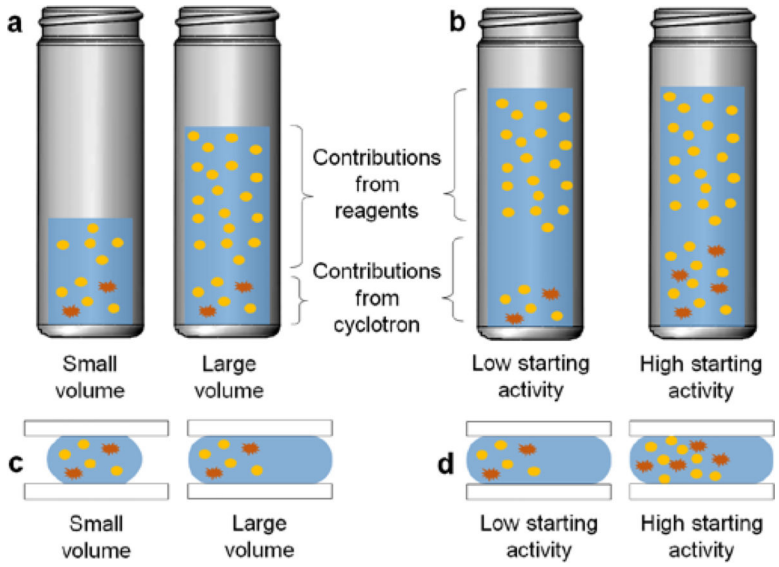

Figure 5: Visual interpretation of the impact of reaction parameters on molar activity at the macro- and microscales.

During the radiofluorination reaction, precursor molecules are labeled with either the radioactive or non-radioactive forms of fluoride (F-18 and F-19) that are present in the reaction mixture. The resulting products cannot be chemically separated, resulting in a mixture of ^{18}F- and ^{19}F-labeled forms of the tracer. (a-b) At the macroscale, reagents are the dominant source of fluorine-19 contamination. Thus, as reaction volume is increased (a), the fluorine-19 contamination is increased, leading to reduced molar activity. As starting radioactivity is increased (b), radioactivity is increased while there is no significant increase in fluorine-19 contamination, and therefore molar activity is increased. (c-d) At the microscale, in contrast, reagents add negligible fluorine-19 contamination compared to that from the cyclotron. Therefore, as reaction volume is increased (c), fluorine-19 contamination remains constant, and molar activity is unaffected. Increasing the starting activity (d) increases both radioactivity and fluorine-19 contamination in proportion, leaving the molar activity unchanged.

Author Manuscript Author Manuscript Author Manuscript Author Manuscript

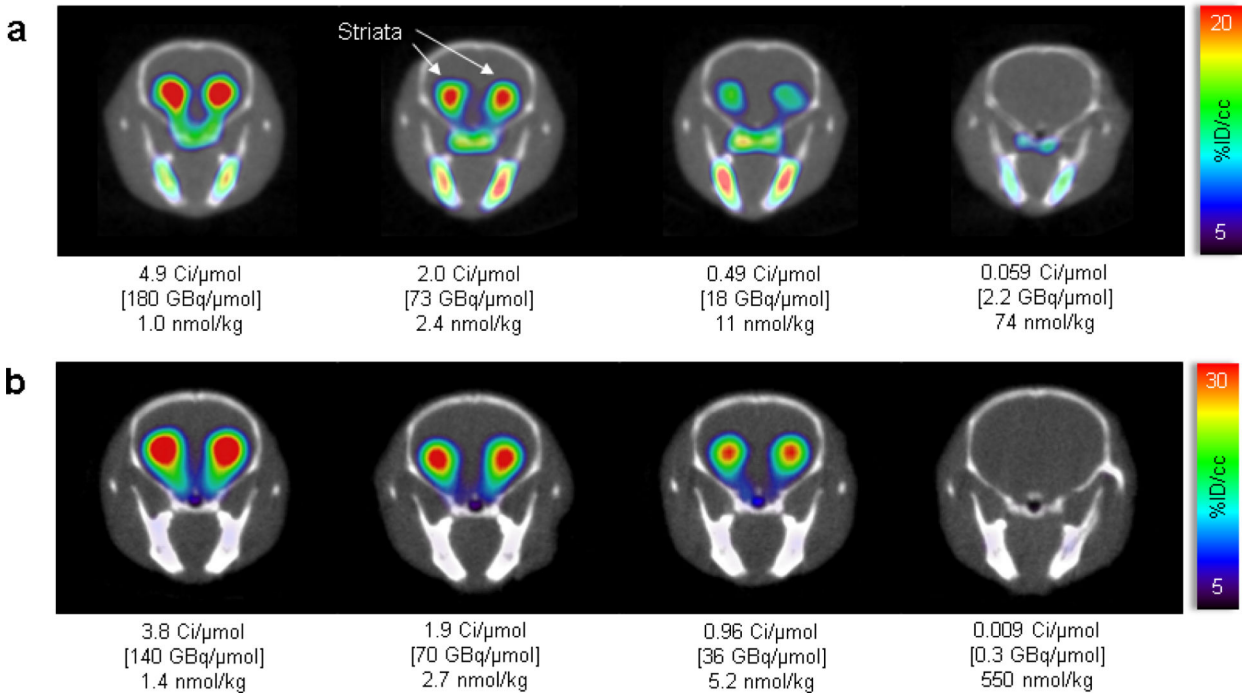

Figure 6: Effect of molar activity on [^{18}F]fallypride PET/CT imaging in mice.

Transverse projections of mouse brain from 10 min static scans after 60 min conscious uptake of [^{18}F]fallypride for two different sets of experiments (a) and (b). Molar activity values are reported at the time of injection, along with the total amount of Fallypride injected per mass of the mouse.